Met Office

Recent results of observation data denial experiments

Weather Science Technical Report 641

24th February 2021

Brett Candy, James Cotton and John Eyre

Met Office

Contents

1 Introduction

The observing network for Numerical Weather Prediction (NWP) is made up of a range of measurement systems, including both surface-based observations and those onboard satellites. Surface-based observations are principally comprised of in-situ measurements such as:

- Reports from meteorological stations of temperature, pressure and wind
- Aircraft reports of temperature, wind and, to a lesser extent, humidity
- Profiles of wind, temperature and humidity from radiosonde ascent

but also include remote sensing observations made from ground-based networks such as total column water vapour estimates from GNSS signals.

Satellite-based observations are made using a wide variety of techniques incorporating active and passive sensors. At the time of writing, these observations are available from over 25 satellites in both low and geostationary earth orbit. In the next few years there are plans to launch new instruments with enhanced capabilities such as those onboard the EUMETSAT Polar System Second Generation Satellites (EPS-SG).

Each measurement system, or observation type, has a dedicated pre-processing scheme to perform several necessary functions prior to the data assimilation step. These functions include:

- Rejection of erroneous observations
- Derivation of auxiliary data required to assimilate the observation
- Applying corrections to remove the observation bias

In addition to utilising new observation types as they become available, increases in forecast impact from the observing network can also come through scientific improvements to the observation pre-processing. Examples of recent new observation types include: MWRI onboard FY-3C and CrIS onboard NOAA-20. Improvements to the observation processing include use of low peaking ATOVS channels over land and use of neutral wind assumption in the scatterometer wind vector forward model.

It is therefore important to regularly measure the relative impact of each type of observing system on NWP forecasts. The main method to do this is to perform a data denial

experiment (hereafter, DDE) in which a full NWP experiment is performed based on operational data usage but with an observation type of interest withdrawn from the pre-processing and data assimilation steps. The resulting forecasts from this experiment are then compared with those produced via a control run (containing all observation types). A full DDE can be computationally expensive, especially if the effects on the ensemble data assimilation system are also measured, and so other methods of estimating impact have been developed. One example is the Forecast Sensitivity to Observation Impact (FSOI) which is a diagnostic generated as part of the data assimilation system and is used routinely at several NWP centres (Langland & Baker, 2004). This method, which uses adjoint sensitivity gradients and actual innovations to estimate the observation impact, has the advantage that the metric can be calculated without removing observations in the system and so can be generated in near real time as part of the tasks within an operational NWP suite. We will show results from the FSOI metric in Section 4 of this report.

The report is set out in the following way. In Section 2 we describe the operational NWP configuration used in these observation impact studies. Sections 3 and 4 show the DDE and FSOI results respectively. Conclusions are presented in Section 5.

2 Operational NWP configuration

At the time of writing the operational configuration at the Met Office is OS43 and the global NWP suite uses hybrid 4D-Var to produce atmospheric analyses at 0, 6, 12 and 18 UTC. Full details of the data assimilation setup can be found in Clayton et al, 2013. The hybrid aspect of the scheme is the use of an ensemble of short-range forecasts to estimate the flow dependent part of the background error covariance (**B**) matrix. Twice daily at 0 and 12 UTC the analyses are used to initialise forecasts with lead times out to six days.

The observations assimilated as part of OS43 are shown in Table 1. The observations are organised into categories that contain instruments of similar types. For instance, all passive microwave instruments. The categories will be used to form the data denial experiments described later. Note that wind profilers and bogus observations around tropical cyclone cores are also assimilated in operations, but these are both small datasets and, although present in the control runs detailed in Section 3, are not tested through any data denial experiments.

Category	Description	Key instruments
Aircraft	temperatures,U,V & RH from aircraft	AMDAR, AIREPS
AMVs	wind vectors from visible and IR imagers onboard geostationary and polar platforms	Geo: MSG/SEVIRI, Himarawi/AHI, GOES/ABI. Polar: AVHRR, MODIS & VIIRS (majority of these obs in high latitude regions)
Geostationary CSR	clear sky radiances from geo IR imagers	MSG/SEVIRI, Himarawi/AHI, GOES/ABI
Ground-based GNSS	total zenith delay, sensitive to total column water vapour and surface pressure from GNSS receivers at a network of stations	Networks in Europe & US
GNSS RO	bending angles sensitive to temperature and humidity	receivers onboard Metop satellites, FY-3C, FY-3D
Hyperspectral IR	radiances sensitive to temperature and humidity	AIRS, CrIS, IASI
MW sounders and imagers	radiances sensitive to temperature and humidity	AMSU-A, ATMS, AMSR2, GMI, MHS
Radiosondes	profiles of temperature, winds and relative humidity	
Scatwind	wind vectors over ocean	ASCAT, WindSat, ScatSat
Surface - land	temperature, relative humidity, pressure and winds from land stations	
Surface - ocean	temperature, relative humidity, pressure and winds over ocean from buoys, ships and rigs	

***Table 1**. Description of the observation categories used in OS43.*

Figure 1 shows the daily average number of “soundings” for each observation category during the two-month period beginning on 15th August 2019 and ending on 15th October 2019. A “sounding” in this context treats a profile or set of channels at the same latitude and longitude location as one statistic. Over 50% of the soundings assimilated are made by satellites operating at microwave and infrared wavelengths. AMVs also contribute to over 10% of the total. If each component of an observation is considered (channels, ascent levels, etc) then a different picture emerges. In this case most of the data assimilated are

from Hyperspectral IR observations, due to the large number of channels associated with each observation (e.g. for IASI typically 65 channels are assimilated, with exact channel usage depending on cloud conditions).

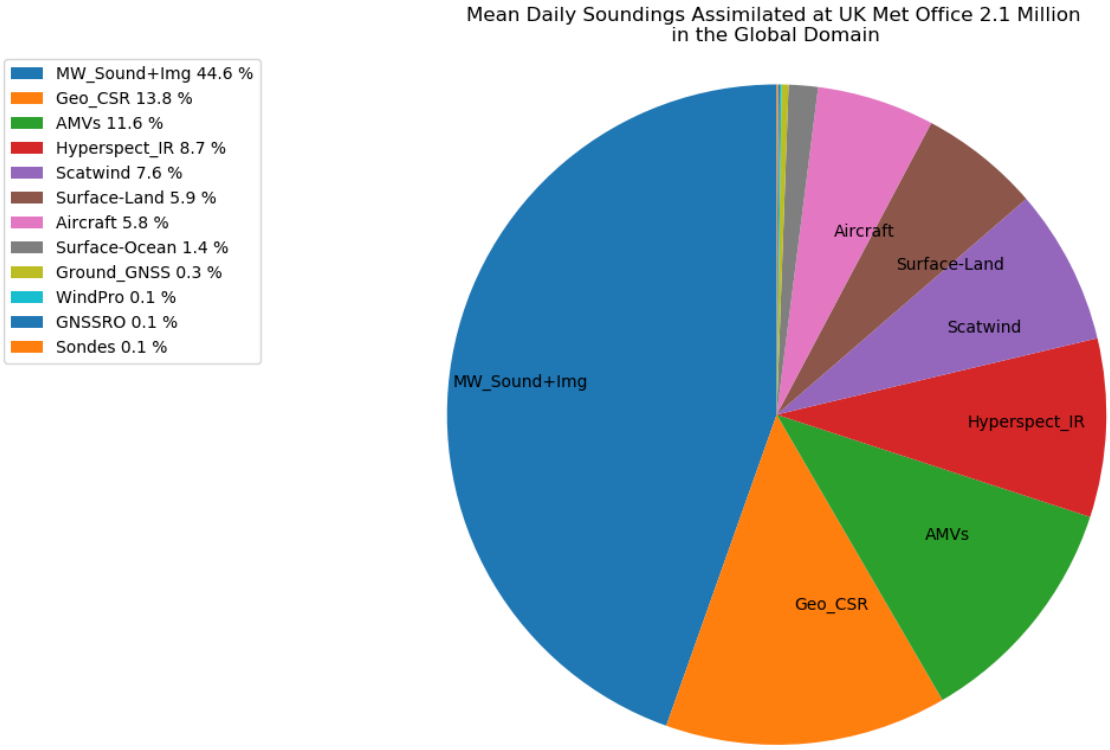

***Figure 1**. Mean number of daily soundings assimilated for each observation category during the period 15th August 2019 to 15th October 2019.*

3 Data Denial Experiments

3.1 Introduction

For each observation category a data denial experiment (DDE) was carried out in the following way. Firstly, a Control run was performed in which the trial version of the operational global NWP suite was run for a period of three months. All observing types were used as detailed in Table 1. The control run differs from the operational configuration in two ways. Firstly, the horizontal resolution of both the analysis and forecast grids are reduced which reduces computational cost. For example, the forecast grid is reduced from 12 km at mid-latitudes to 40 km. In addition to this the flow dependent part of **B**, the background error matrix used within 4D-Var, is determined from archived ensemble data. This change avoids the requirement of running the ensemble task. The period of the Control run is from 15th August 2019 – 15th November 2019. A series of DDEs was then performed and these were identical to the Control with the exception of the removal of the observation category of interest from use in the assimilation step. To determine the observation impact of each DDE the resulting "errors" in the forecasts are calculated using two sources of verification data. These are observations made at the forecast validity time and, in addition, an independent NWP analysis (ECMWF operations). Although in the rest of this paper the term forecast errors will be used it is important to note that these are computed from differences between two estimates of truth, the forecast and verifying dataset, each of which contain errors. The DDE forecast "errors" are then compared to the control run. An example is shown in Figure 2. This shows the forecast impact for the Microwave Sounder & Imager DDE, using the standard scorecard format. The scorecards show the change in root mean square forecast error (as a percentage) for a variety of key forecast variables through the troposphere. For verification against observations these are: winds at 10 m , 850 hPa, 500 hPa and 250 hPa; temperatures at 2 m, 850 hPa, 500 hPa and 250 hPa; geopotential heights at 850 hPa, 500 hPa and 250 hPa; pressure at mean sea level. Whist the surface parameters use station reports as verifying observations, above the surface layer the verifying observation type used depends on the specific variable and level, in an effort to use the observation type with the lowest errors. These are shown on the right column of the scorecard and are made up of radiosondes, AMDARS and AMVs. The results are also split into 3 latitude bands: NH: 90°N - 20°N; TR: 20°N - 20°S & SH: 20°S - 90°S.

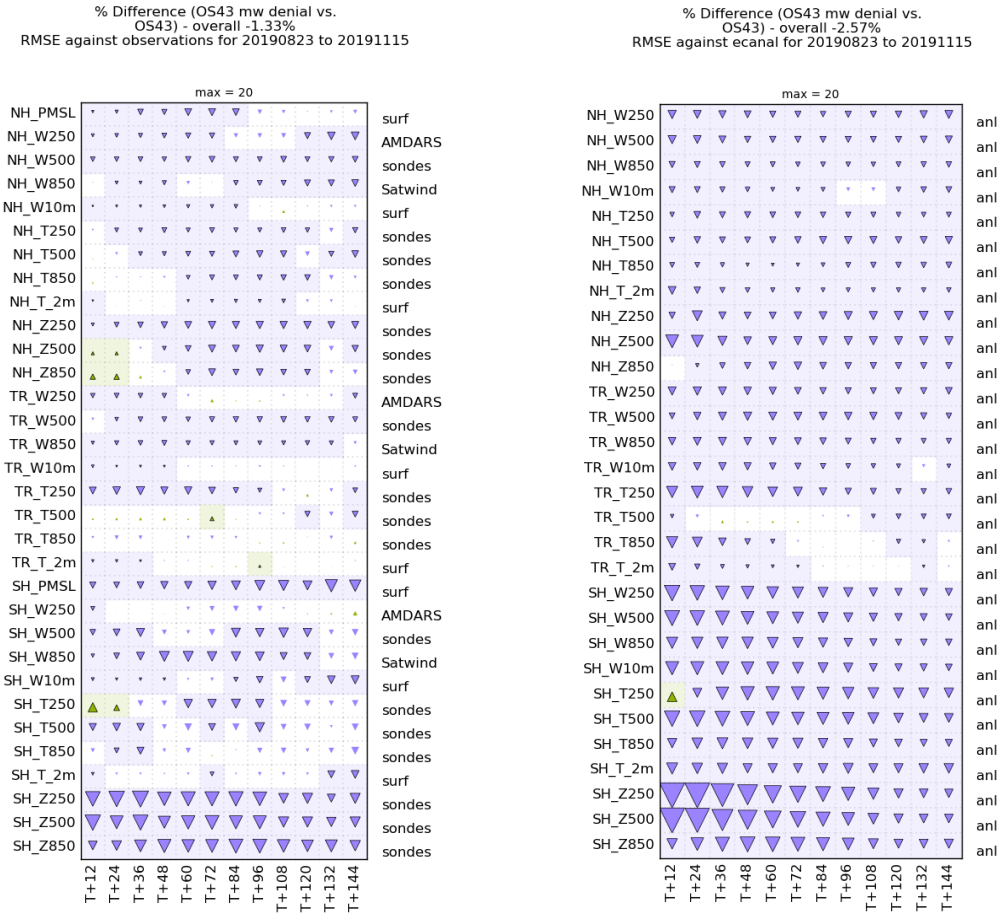

***Figure 2**. The percentage change in root mean square forecast error for the Microwave data denial experiment. Left Panel: changes verified using observations. right panel: changes verified using ECMWF analyses. The description of each forecast variable is discussed in the text of the report. Forecast degradations (relative to the control run) are denoted by downward triangles, whilst shading denotes statistical significance.*

Surface pressure is not used when verifying against analyses, due to differences in how this diagnostic is computed between Met Office and ECMWF NWP schemes. For each of the variables within the scorecard forecast errors are determined at 12 hour intervals from T+12 to T+144.

Forecast degradations (relative to the control run) are denoted by downward triangles, whilst shading denotes statistical significance. It is important to note that the results are in terms of a DDE; that is to say that a forecast degradation demonstrates that the observations removed are providing a forecast benefit. It can be seen that the Microwave DDE results in significant degradation over most of the variables and forecast times. Overall, the mean change in forecast error is found to be -1.33 % when verified by observation and -2.57 % when verified by ECMWF analyses. The largest detriments are found in the Southern Hemisphere geopotential height forecasts, with values of 27% at T+12.

3.2 Results

Figure 3 summarises the results of each DDE by presenting the mean scorecard changes for each observation category. The full scorecards for each DDE can be found in Appendix 1.

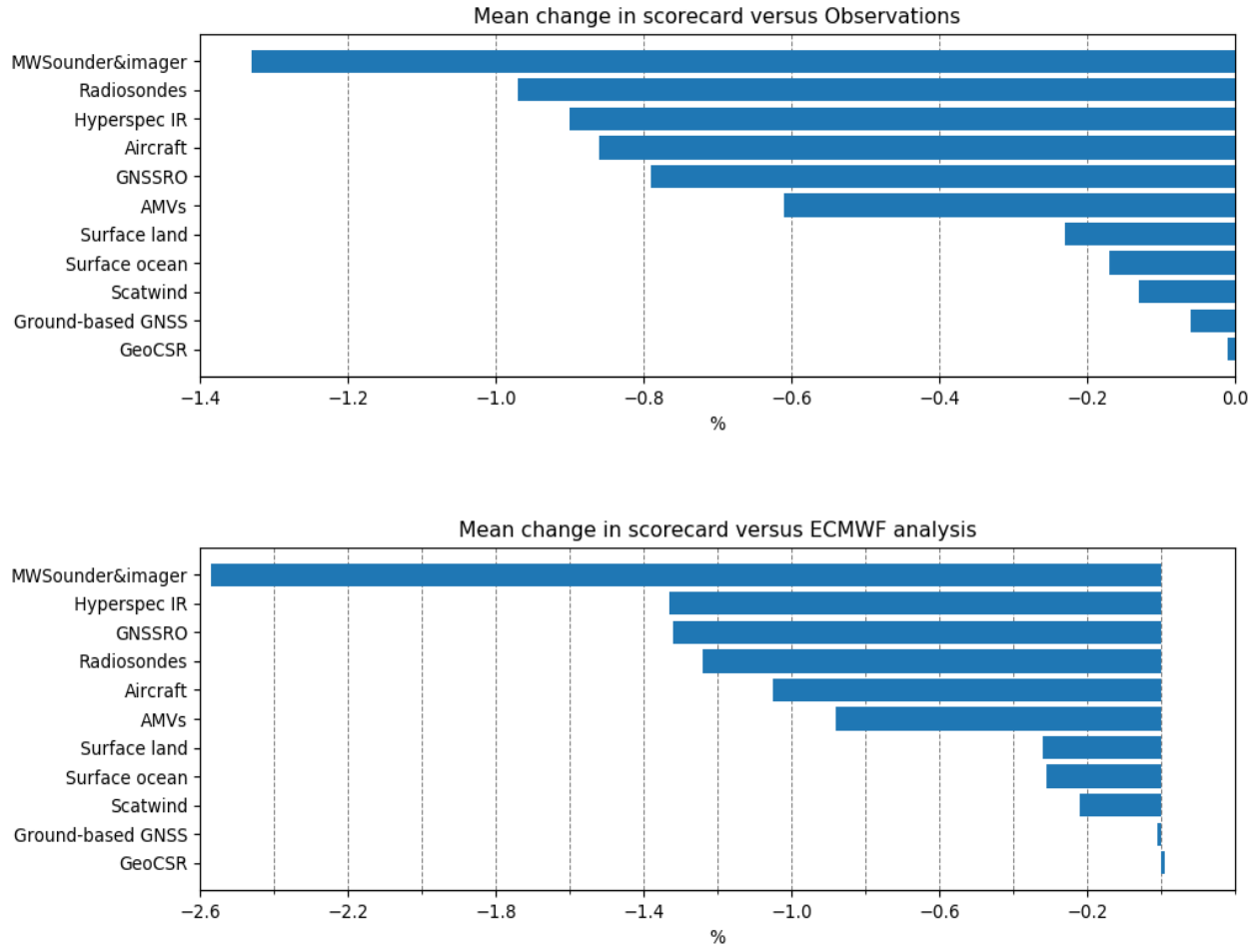

Figure 3. *The mean change in data denial scorecard for each observation category. Top panel: verified using observations, bottom panel: verified using ECMWF analyses.*

In general, the impacts are larger when verified using ECMWF analyses. A possible explanation for this is that the conventional observing network (with which most of the parameters are verified if using observations; an exception is AMVs for verifying 850 hPa winds) does not have uniform coverage across the globe. Large changes to the forecast error may occur in the Southern Ocean and this may not be adequately sampled at the locations of the verifying observations. Nearly all observing categories show a negative

mean change denoting that the forecasts are degraded when the category is removed. A notable exception is the use of clear sky radiances from geostationary orbit (GeoCSR). Despite accounting for over 10% of observation usage (Figure 1) this category shows almost neutral impact, according to the scorecard metric. There is other evidence, however, that this category improves the short-range humidity fields. Within the GeoCSR DDE, a degraded fit of up to 2% was noted for the O-B fits of CrIS and AMSU channels sensitive to humidity.

The categories with the largest detriment in forecast quality when withdrawn are those which include sounding information on temperature and humidity: microwave, hyperspectral infra-red sensors and radiosondes. Radio occultation measurements, AMVs and aircraft also appear important.

Figure 4 Shows the RMS forecast error for temperature at T+48 hours (a time chosen when the forecast error starts to dominate over the errors associated with the verifying source, in this case radiosondes). Changes to the forecast error below 200 hPa are positive, showing that the removal of the various observation categories has degraded the forecast in the troposphere. Above 200 hPa this positive trend continues for most of the observation types shown. In particular, the results are dominated by the large degradation in the GNSS RO DDE. This is seen in both hemispheres and is largest in the Southern Hemisphere with a peak degradation of 15%. It suggests that GNSS RO data are extremely beneficial in the stratosphere. In contrast there is a suggestion that Hyperspectral IR observations degrade the upper level temperature forecasts, as there is evidence that the temperature forecasts improve above 200 hPa in the Hyperspectral IR DDE.

Similar plots are shown in Figure 5 for wind speed. Here degradations can be seen through the troposphere, for both radiance and AMV DDEs. In particular, around the jet region where degradations due to the withdrawal of the observations are up to 1.5%. These results show the ability of the data assimilation system to extract dynamical information from the microwave and infra-red radiances. With current research in these two data types focusing on all sky scenes, the use of which helps to improve the forecast wind field (e.g. Migliorini and Candy, 2019; Pavelin, 2020), we hope to further benefit the wind field in the future. It is also worth noting that the largest change in AMV DDE when compared to the other major observation categories is for tropical windspeeds in the upper troposphere (not shown).

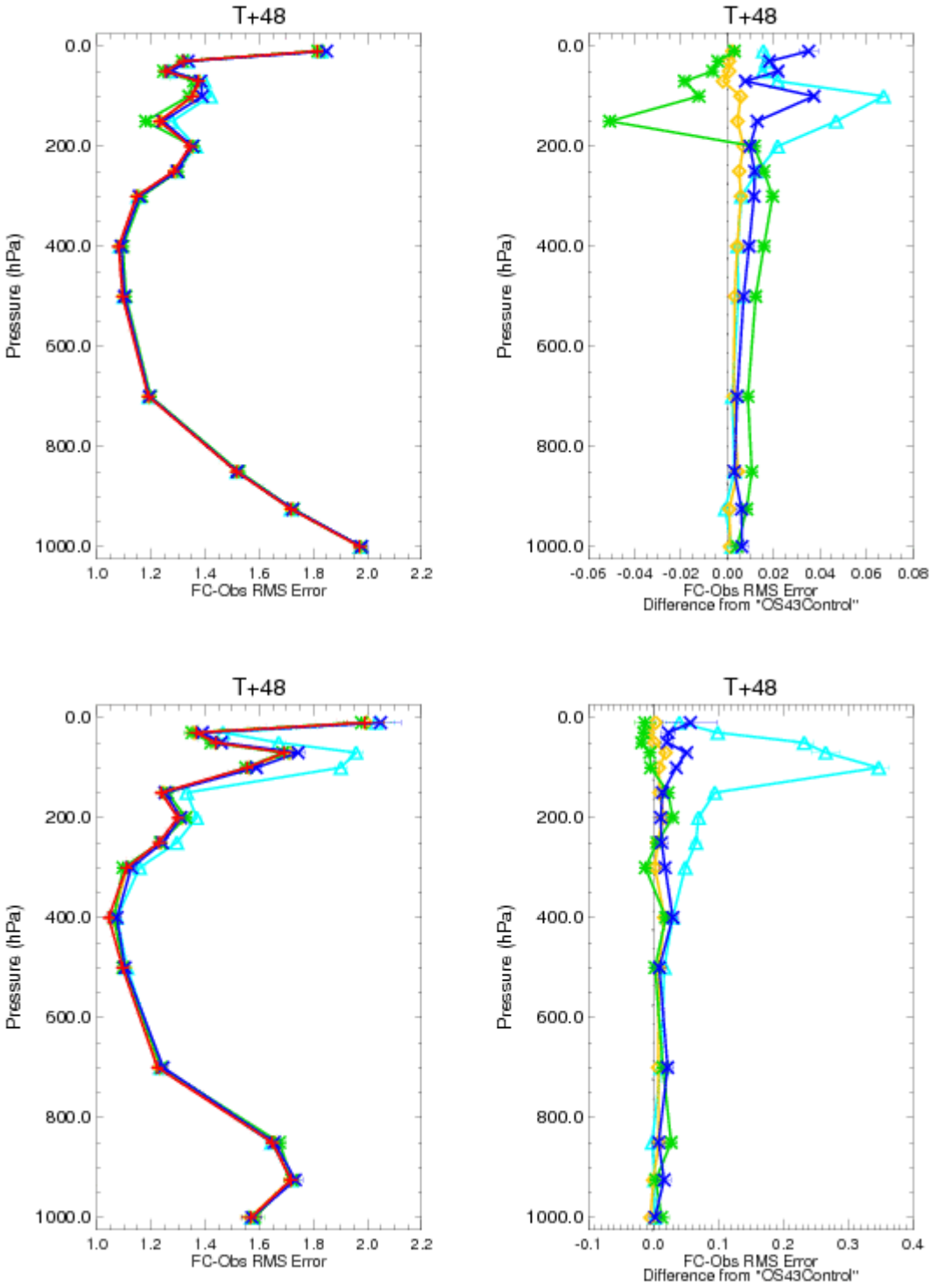

***Figure 4**. Profiles of the T+48 temperature RMS forecast errors and the differences between experiment and control for various DDEs. Top row shows results for the Northern Hemisphere and bottom row for the Southern Hemisphere. Key: light blue: GNSS RO DDE, dark blue: MW DDE, green: Hyperspectral IR, orange: AMVs DDE.*

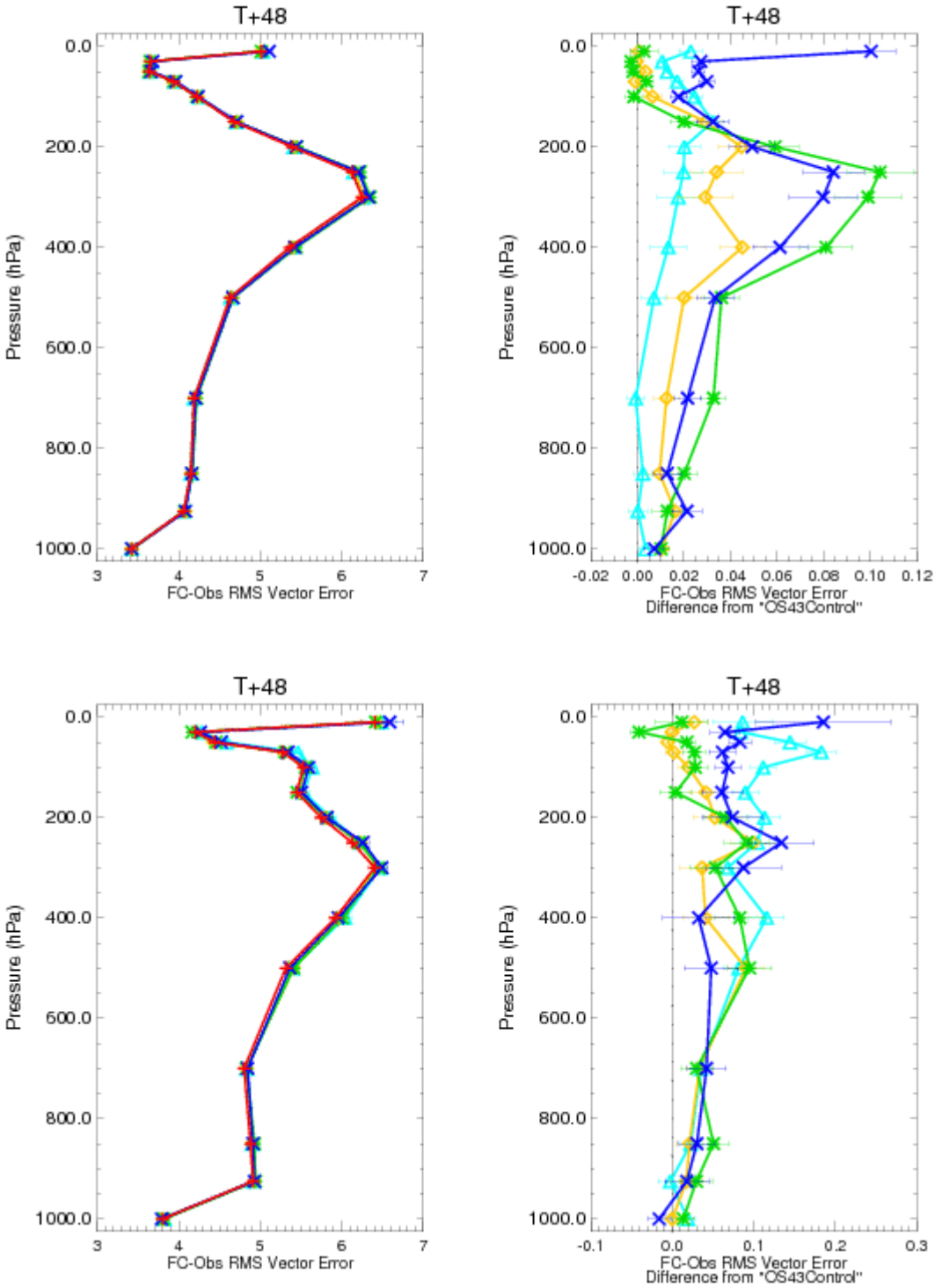

***Figure 5**. Profiles of the T+48 windspeed RMS forecast errors and the differences between experiment and control for various DDEs. Top row shows results for the Northern Hemisphere and bottom row for the Southern Hemisphere. Key: light blue: GNSS RO DDE, dark blue: MW DDE, green: Hyperspectral IR, orange: AMVs DDE.*

3.3 Continued Impact of POES

The POES (Polar Operational Environmental Satellite) system contains the US contribution to polar weather satellites in the early afternoon orbit. Although superseded by a new generation of satellites and instruments in 2017, with the launch of NOAA-20, three 5th generation POES satellites still operate and provide data in near real time to NWP centres. These are NOAA-15, 18 and 19. All three platforms still provide AMVs (from the AVHRR instrument) and AMSU measurements. The HIRS IR sounding instrument is no longer used from these or indeed any platforms in Met Office operations. The percentage of AMVs supplied by the POES satellites is less than 1% of the total AMVs used at each assimilation step, which is not surprising given that the geostationary satellites make up the main source of this observation category.

Due to the length of service in space, the microwave sounding instruments onboard the POES satellites now have at least two channels which have failed or are outside of specification with regard to noise (Table 2). Despite this, results of a DDE which examines the loss of these microwave and AMV observations from NOAA-15,18,19 is shown in Figure 6. The scorecards show that many fields are degraded when the NOAA platforms are removed. In particular, tropical winds and height fields in the southern hemisphere. For both these forecast fields detriment is seen in both scorecards (versus observations and ECMWF). Figure 7 highlights that the majority of short-range fits between the NWP model forecasts and other observations have degraded. In particular, the fits of low-level AMSU channels from the Metop satellites have degraded by around 4%. Overall, these results show that the use of observations from POES satellites still results in a significant benefit to NWP forecasts.

	NOAA-15	NOAA-18	NOAA-19
AMSU-A channels			
1	*	*	*
2	*	*	*
3	*	*	*
4	●	●	●
5		●	●
6		●	●
7	●	●	
8	●	●	
9	●		●
10	●	●	●
11		●	●
12	●	●	●
13	●	●	●
14		●	●
MHS/AMSU-B channels			
1			*
2			*
3			●
4			●
5			●

Table 2. *Working microwave channels on NOAA-15,18,19 assimilated during the data denial period. Asterix denotes channels used for pre-processing of surface and cloud information (1D-Var in OPS), but not used in the 4D-Var full assimilation task.*

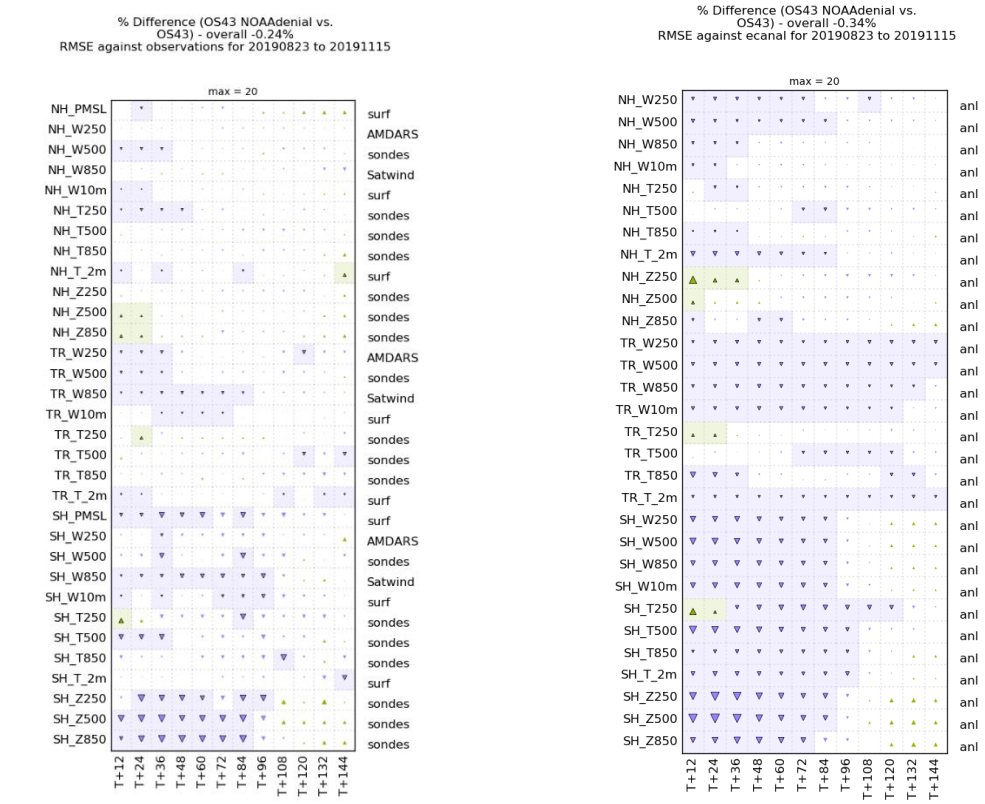

Figure 6. *The percentage change in root mean square forecast error for the NOAA-15,18,19 AMSU and AMV data denial experiment. Left Panel: changes verified using observations. right panel: changes verified using ECMWF analyses.*

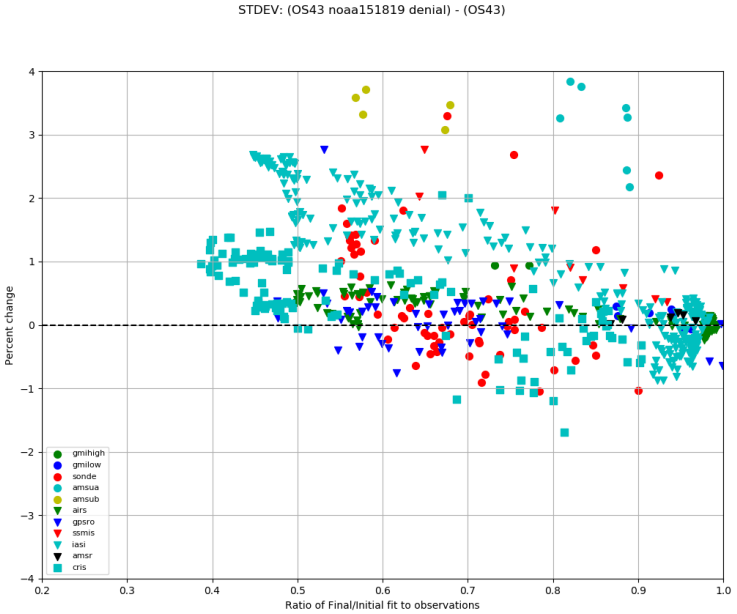

Figure 7. *A summary of the percentage change in fit of O-B for each observation type between the NOAA-15,18,19 DDE and Control. Positive changes on the Y-axis signify degraded fit in the DDE. Each point from a given observation type represents a channel (for radiances) or layer (for radiosondes).*

3.4 Verification of Tropical Cyclone Tracks

The period of the data denial experiments includes a large part of the tropical cyclone season in the northern hemisphere. Tropical cyclone positions are disseminated by regional hurricane centres and inspection of these data shows that there are tropical cyclones present during the trial period in the main regions where these severe storms occur in the northern hemisphere. The tropical cyclone positions can be used to verify the performance of the NWP system in modelling the evolution of these storms within forecasts. In particular, the forecast track error is of most interest and further details on how the validation is performed can be found in Heming (2017). Results are shown below for two of the observation categories which potentially can provide beneficial data to the forecast: AMVs and scatterometer winds. Both these observation categories show large forecast detriments to the tropical wind field in the relevant DDEs. For example, in the case of AMV withdrawal at T+24 the 250 hPa winds are found to degrade by over 1% when verified against AMDARs. Despite this Figures 8a and 8b show that the impacts on tropical cyclone forecast track errors when the observation categories are withdrawn are small compared to the associated uncertainties as expressed by the error bars. Track errors are degraded at T+12/24 in the AMV DDE and at T+0/12 for the scatterometer DDE, but the changes are not statistically significant.

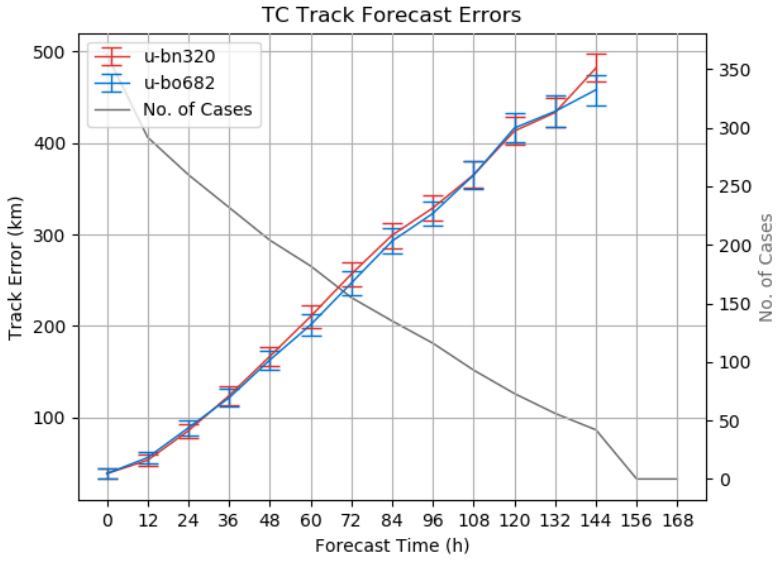

***Figure 8a**. The tropical cyclone track error against forecast time for the control run (red) and the AMV DDE (blue).*

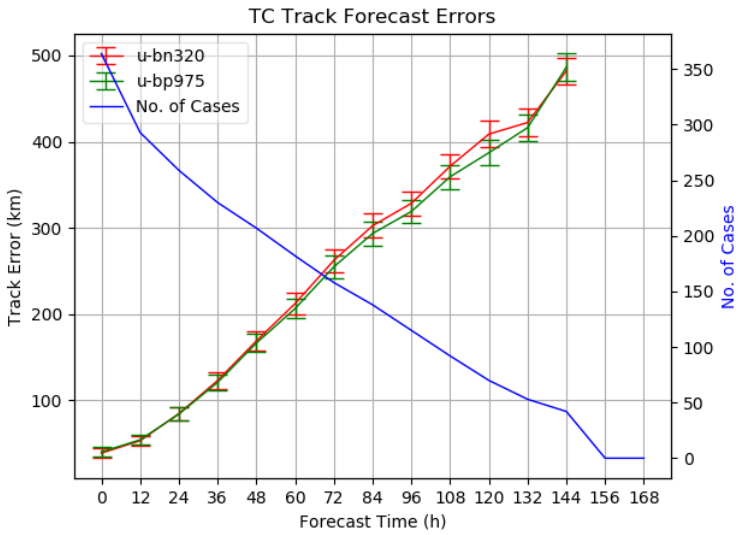

Figure 8b. *The tropical cyclone track error against forecast time for the control run (red) and the scatterometer DDE (green).*

When the uncertainties are considered there are no significant impacts on track errors for any of the observation category DDEs. It suggests that more cases are required, through the accumulation of forecasts over several hurricane seasons. Also, because of the small-scale nature of tropical cyclones, it is also likely to be important that the data denial trials are run at higher (operational) horizontal resolution.

3.5 A Data Denial Experiment including withdrawal from the ensemble

For the DDEs described above the impact on the deterministic data assimilation has been assessed and the effect on the ensemble part of the data assimilation has been ignored. In the hybrid data assimilation method, as is used in the Met Office global NWP system, the ensemble is used to contribute part of the background error covariance or **B** matrix. It is too computationally expensive to run the ensemble in each data denial experiment and so the results above do not measure any impact from the change in **B.** For small forecast impacts this is probably fine, but in the case of the Microwave DDE or radiosonde DDE, potentially a large change to the magnitude of **B** is not properly described in these experiments. In order to test whether the withdrawal of data on the ensemble has an additional effect, a trial was performed running an additional microwave DDE, including the full ensemble data assimilation and with all microwave data withdrawn in both the deterministic and ensemble parts. This is referred to below as a FullDDE. Because of technical issues this was

performed for the period 1st December 2019 to 31st January 2020. The results below are compared to a DDE for the same period which is configured in an identical manner to the earlier trial runs, that is using operational ensemble data in both experiment and control. This is referred to as an UncoupledDDE since it is not fully coupled to the ensemble and therefore the hybrid DA scheme. The headline score card results are shown in Table 3 and these show that the results are similar for the two types of DDE, with the FullDDE showing a slightly higher detriment. Figure 9 compares the change in forecast errors for the two types of DDE. There is evidence that the detriments further into the forecast range are greater for the FullDDE, particularly for the wind and height fields. It is worth pointing out that only part of the contribution to the covariance matrix has been examined in this FullDDE experiment; no tests have been performed accounting for data denial effects in the climatological part of the background error covariance matrix. Estimating the climatological **B** matrix is a complex procedure (e.g. one of the methods described in Bannister, 2008) and beyond the scope of the work presented here**.**

Type of Trial	**Scorecard Change**	
	Versus observations	**Versus ECMWF**
FullDDE	-0.96	-1.95
UncoupledDDE	-0.77	-1.83

Table 3*. A comparison of the headline score card change for the FullDDE (including ensemble effects) and the UncoupledDDE for Winter 2019.*

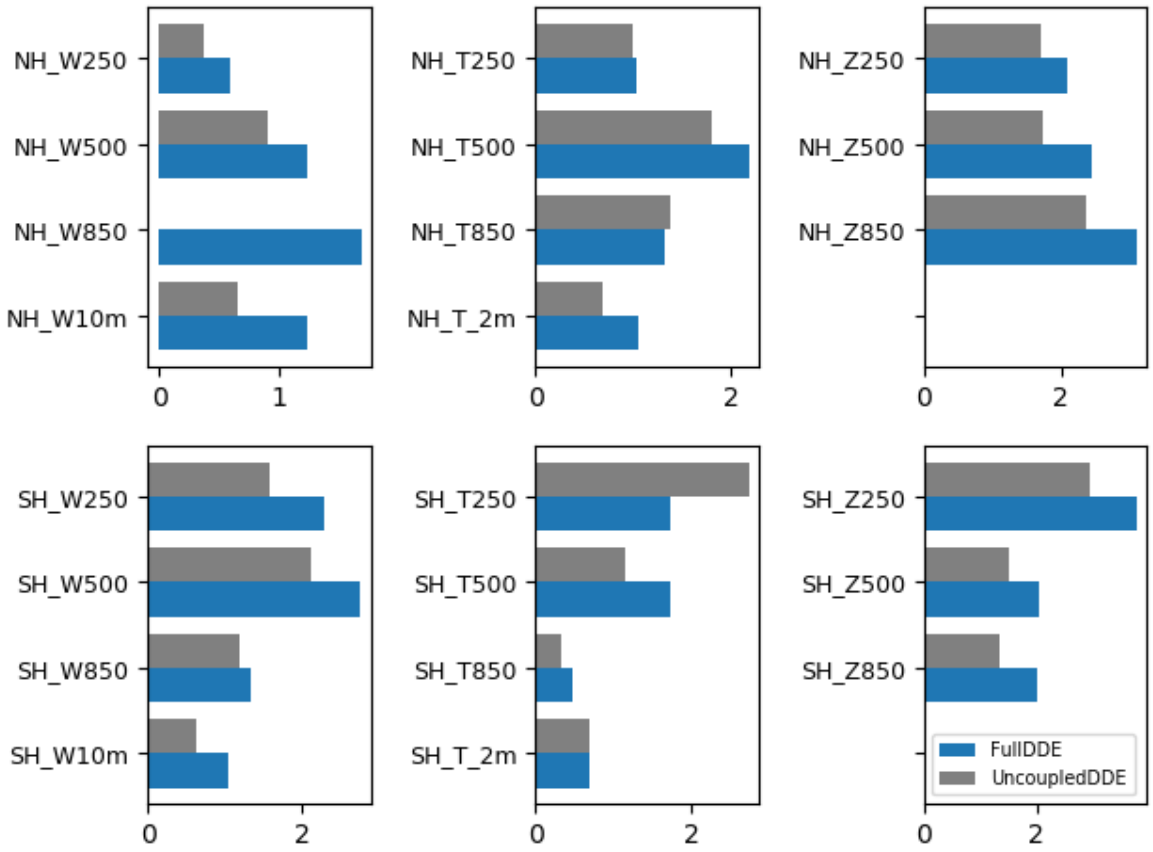

***Figure 9**. The percentage change in forecast error for the FullDDE (including ensemble effects) and the UncoupledDDE for extratropical forecasts at T+96. Top row: Northern hemisphere extratropics; Bottom row: Southern hemisphere extratropics.*

4 FSOI Results

Figure 10 shows FSOI results for September 2016 and for the period 15th August – 15th October 2019, the latter representing the first 2 months of the DDE. The earlier period represents the scores during OS37, when a previous round of DDEs was carried out. Comparing the two periods it can be seen that in both cases the passive sounding data (both IR and microwave) are the top two categories in the FSOI diagnostic. In 2019 the MW category yields the highest impact, whereas for the earlier period it is the Hyperspectral IR category. When comparing the DDE impact scores with FSOI the order of impact is similar, though not identical. A notable difference is GNSS RO which is higher in order of impact for the DDEs. Looking at the time series (an example is shown in Figure 11 for AMSU-A, ATMS, CrIS and AMVs) the main changes over the period 2016 to 2019 are around a 2% increase

in relative impact for each of the instrument types. The increase in AMSU-A is mainly brought about through reintroduction of NOAA-18 and improvements to thinning (early

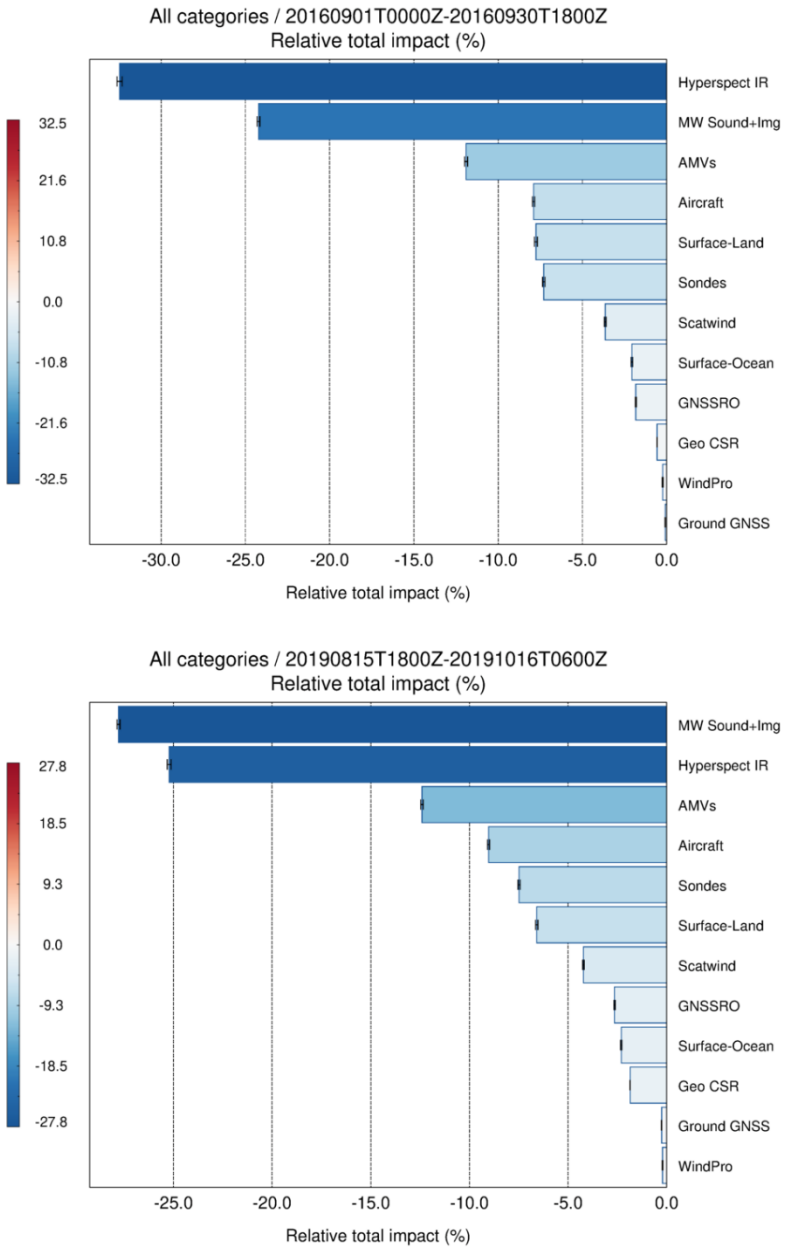

Figure 10. *FSOI results by observation category for (top panel) September 2016 and (lower panel) Autumn 2019.*

2018), although more recently the impact drops slightly (which is also seen for IASI). For the other three observation types benefits are increased through use of new instruments (e.g. introduction of NOAA-20 in mid- 2018 and GOES-16 AMVs in May 2018 and Nov 2019)

Figure 12 expresses the FSOI results in terms of platforms and the continued high importance of the Metop and NOAA platforms can be seen. Notice too that for this period we also can see the benefit of CMA observations from the FY-3 series of satellites, operating in a polar orbit. Currently in OS43 the FY-3 platforms provide microwave sounding/imaging capabilities and also GNSS RO observations.

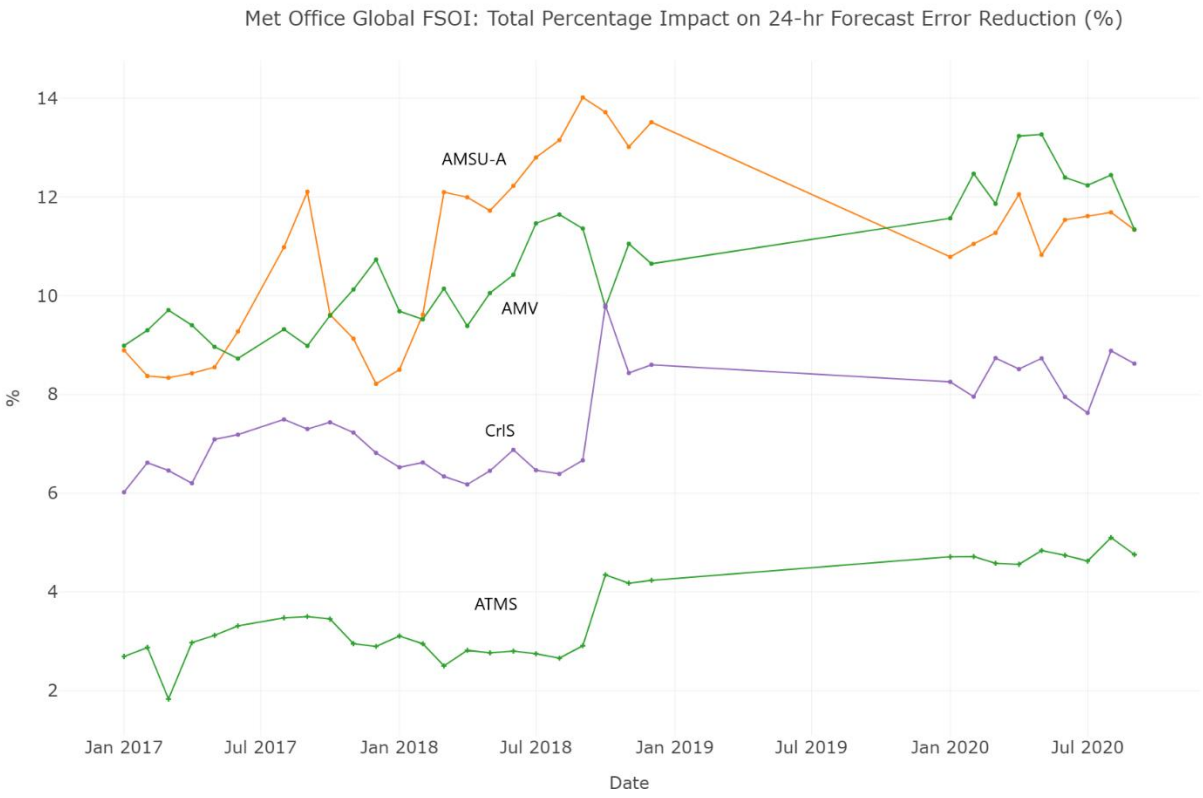

***Figure 11**. Time series of the FSOI impact for AMSU-A, CrIS, ATMS and geostationary AMVs. Impacts are unavailable for January to December 2019 due to technical issues*

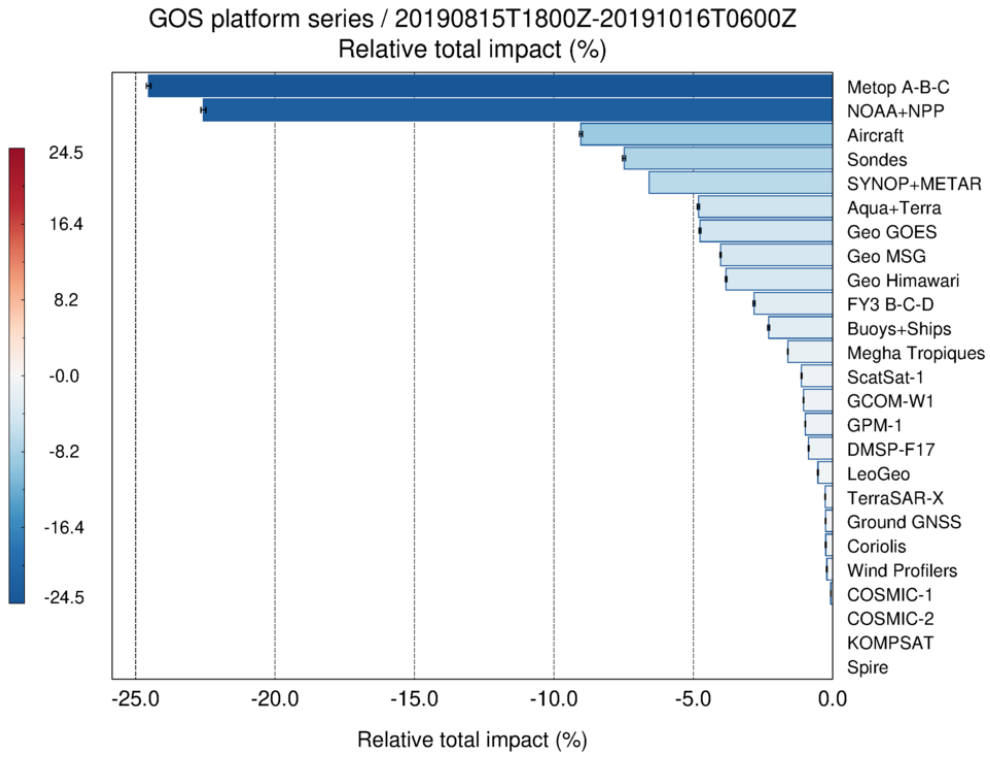

Figure 12 *The FSOI impact by platform for the Autumn 2019 DDE period*.

5 Conclusions

A series of data denial experiments has been performed for all of the major observation categories used in the Met Office global NWP system. The system is based on OS43, the operational configuration in use between December 2019 and December 2020. Results show that the assimilation of radiances (from both microwave and infra-red instruments) and radiosonde profiles are still extremely important. Other categories which also yield a large detriment in forecast when withdrawn include AMVs, observations from commercial aircraft and GNSS radio occultation. FSOI results accumulated over the same period (and configuration) in autumn 2019 reflect the DDE results to a large degree. For instance, the FSOI total accumulation shows that over 50% of the impact comes from the assimilation of radiances. A notable exception is GNSS radio occultation. The FSOI diagnostic for this observation suggests that its contribution is less (8th out of 12 categories) than is found in the data denial experiment.

These results are generally in line with a recent study at ECMWF (Bormann et al., 2019). This study also examined the impact of the main observation categories through a series of DDEs within the ECMWF global NWP system. Although the trial periods are different, the

ECMWF study also found a strong impact from the microwave data and conventional data (which in their categorisation included radiosondes). The importance of GNSSRO data in the upper troposphere/stratosphere was also noted. By contrast, the medium-range impact of microwave data on the tropospheric wind forecast appears stronger at ECMWF, especially in the Southern Hemisphere. This is most likely due to the extensive use of all-sky assimilation at ECMWF, particularly for the water vapour sounders such as MHS. It is also worth noting that the ECMWF study examined two different time periods in order to gauge the seasonal effect. This appears to be important in the Northern Hemisphere for the relative impacts between conventional and satellite data. Future studies should consider investigating if this result can be repeated in the Met Office NWP system.

The impact of observation withdrawal on the forecast of tropical cyclone tracks has also been investigated as part of this work. In the period examined, autumn 2019, we find no statistically significant impact on the tracks from the individual removal of any of the observation categories.

Despite their length of time in orbit, the POES era satellites (NOAA-15, NOAA-18 & NOAA-19) continue to provide observations in near real time. A dedicated experiment investigating the loss of the POES instruments highlighted the continued benefit to forecasts from these observations. This result is also reflected in the FSOI. The benefit of the FY-3 series of polar satellites, as shown in the FSOI diagnostics is also noted.

Data usage in NWP is continually evolving, as new science is exploited, and as new instruments become available in near real time. Comparisons of the change in FSOI over the last four years have highlighted the increases in impact for certain categories as new instruments start providing data e.g. the CrIS hyperspectral sounder on NOAA-20. Future impact studies are likely to see the continued increase in importance of GNSS RO data as new receivers become available. Other changes of note in the short-term for future contribution to impact studies include wind profiles from the Aeolus LIDAR (Stoffelen et al., 2005), increased use of Metop-C data and additional sounding from radiosondes through use of the descending part of the profile.

Acknowledgements

The impacts discussed in this report arise from the results of many data denial experiments. The authors thank the following people who helped run the experiments: Neill Bowler, Fabien Carminati, Amy Doherty, Chawn Harlow, Owen Lewis, Stefano Migliorini, Ruth Taylor and Christopher Thomas.

References

Bannister, R.N. (2008). A review of forecast-error covariance statistics in atmospheric variational data assimilation. I: characteristics and measurements of forecast-error covariances. Quarterly Journal of the Royal Meteorological Society, 134, 1951-1970.

Bormann, N., Lawrence, H. and Farnon, J. (2019). Global observing system experiments in the ECMWF assimilation system, ECMWF Technical Memo 839.

Clayton, A.M., Lorenc, A.C. and Barker, D.M. (2013). Operational implementation of a hybrid ensemble/4D-Var global data assimilation system at the Met Office. Quarterly Journal of the Royal Meteorological Society, 139(675), 1445-1461. https://doi.org/10.1002/qj.2054

Heming, J.T. (2017) Tropical cyclone tracking and verification techniques for Met Office numerical weather prediction models. *Met. Apps*, 24: 1-8.

Langland, R. H. and Baker, N. (2004). Estimation of observation impact using the NRL atmospheric variational data assimilation adjoint system, Tellus A: Dynamic Meteorology and Oceanography, 56:3, 189-201

Migliorini, S. and Candy, B. (2019). All-sky satellite data assimilation of microwave temperature sounding channels at the Met Office. Quarterly Journal of the Royal Meteorological Society. doi: 10.1002/qj.3470

Pavelin, E. (2020). Initial trials of infrared all-sky radiance assimilation, Satellite Applications Tech Memo 109. Internal to Met Office.

Stoffelen, A., Pailleux, J., Källén, E., Vaughan, J.M., Isaksen, L., Flamant, P., Wergen, W., Andersson, E., Schyberg, H., Culoma, A.and Meynart, R. (2005). The Atmospheric Dynamics Mission For Global Wind Field Measurement. *Bull. Amer. Meteor. Soc.*, **86**, 73–88, https://doi.org/10.1175/BAMS-86-1-73.

Appendix 1. Scorecards for the data denial of each observation category

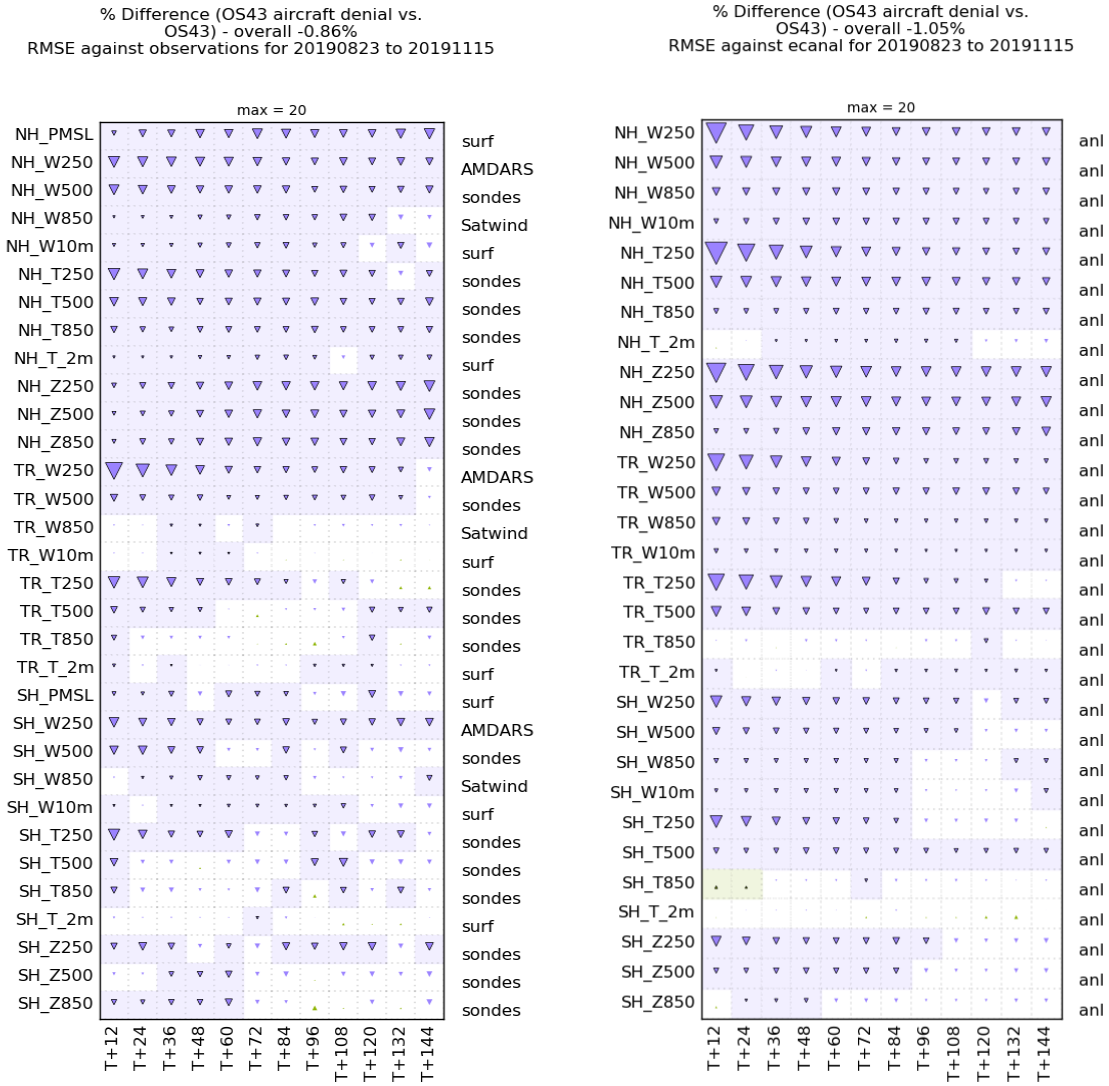

Figure A1 *The change in root mean square forecast error for the aircraft data denial experiment. Left Panel: changes verified using observations. right panel: changes verified using ECMWF analyses.*

The largest forecast detriment found in the aircraft denial was 11% for T+12 NH 250 hPa temperature (verified by ECMWF analyses).

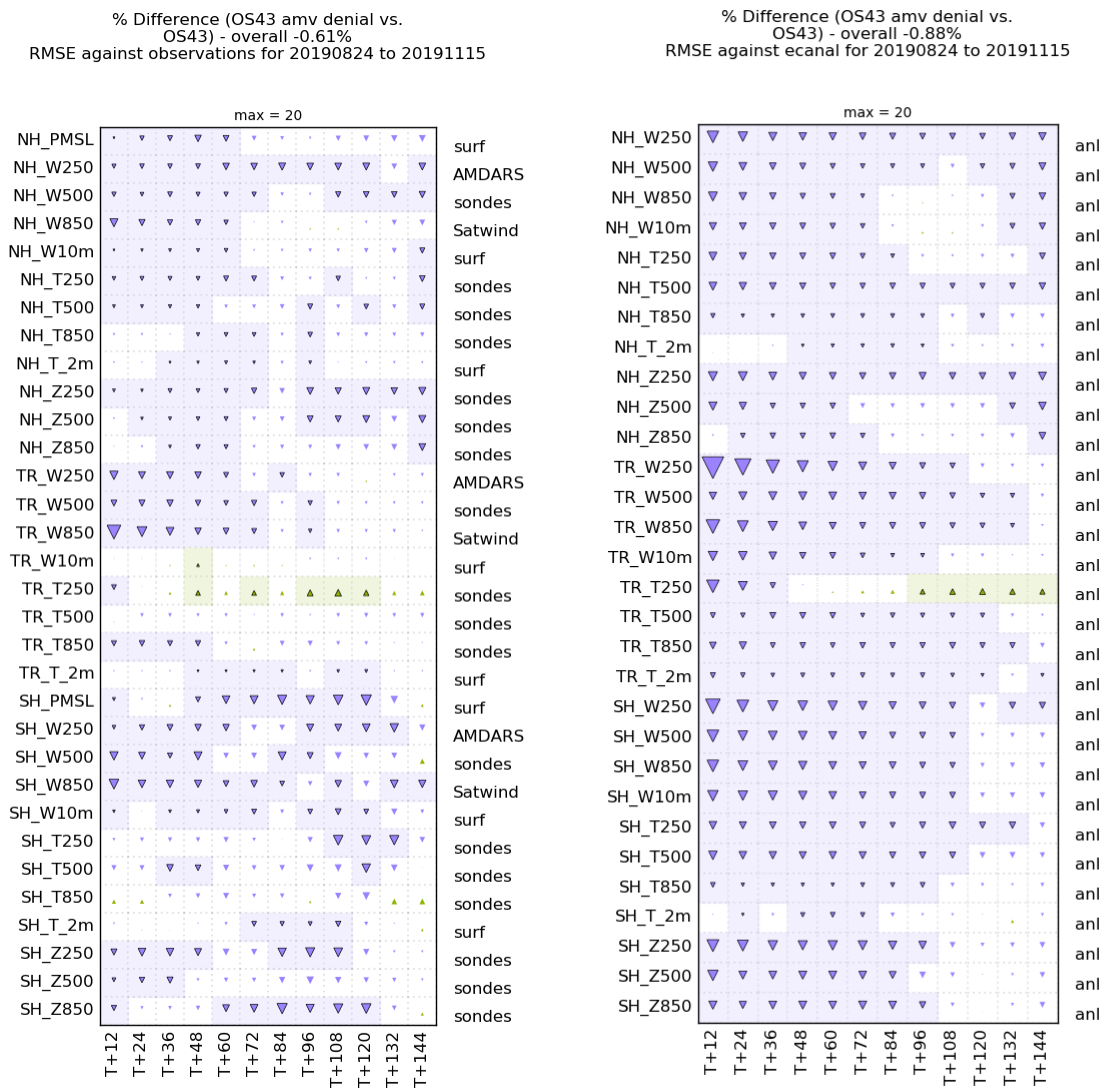

Figure A2 *The change in root mean square forecast error for the AMV data denial experiment. Left Panel: changes verified using observations. right panel: changes verified using ECMWF analyses.*

The largest forecast detriment found in the AMV denial was 10.4% for T+12 TR 250 hPa winds (verified by ECMWF analyses).

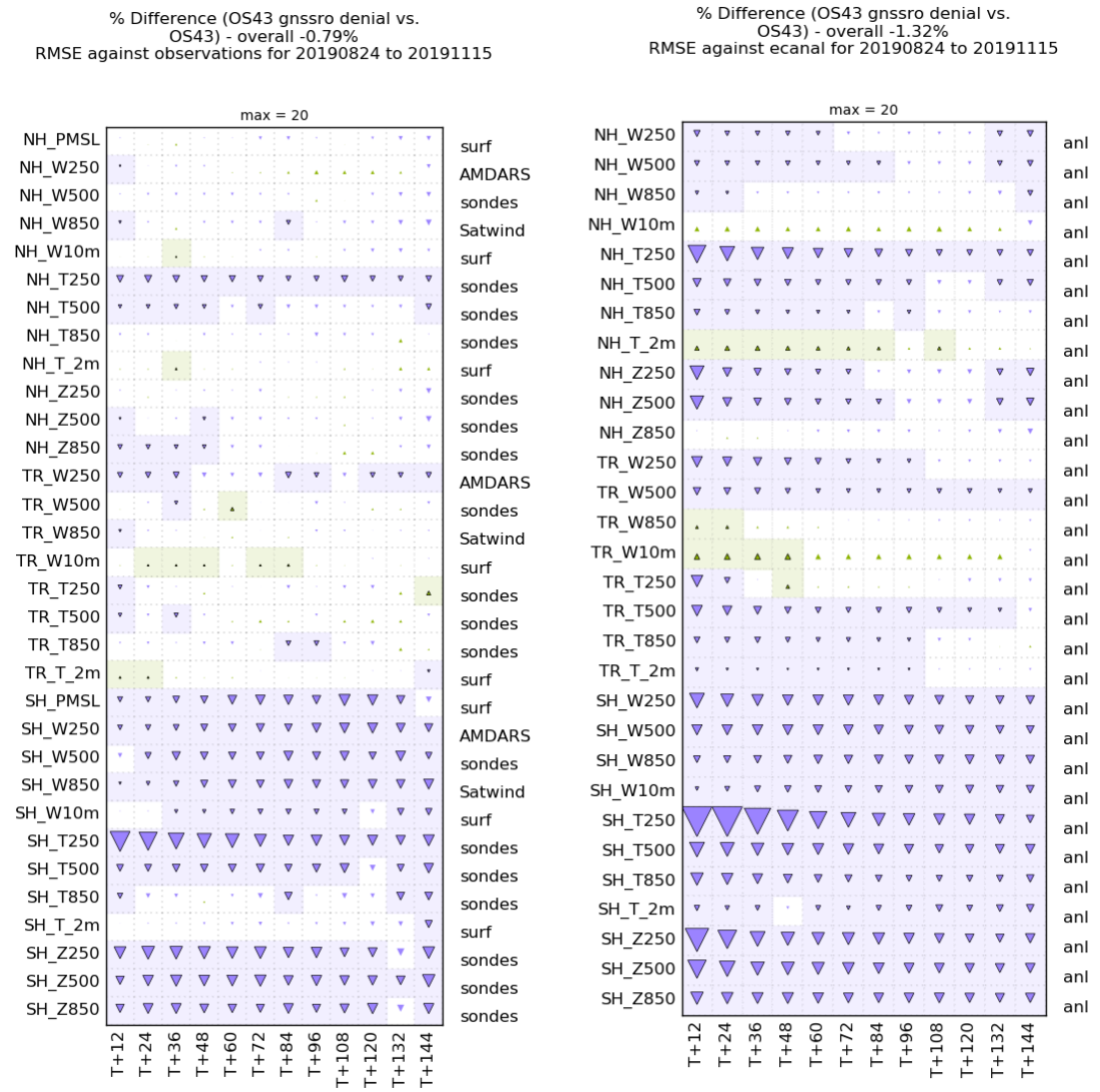

Figure A3 *The change in root mean square forecast error for the GNSS RO data denial experiment. Left Panel: changes verified using observations. right panel: changes verified using ECMWF analyses.*

The largest forecast detriment found in the GNSS RO denial was 37.4% for T+12 SH 250 hPa temperature (verified by ECMWF analyses).

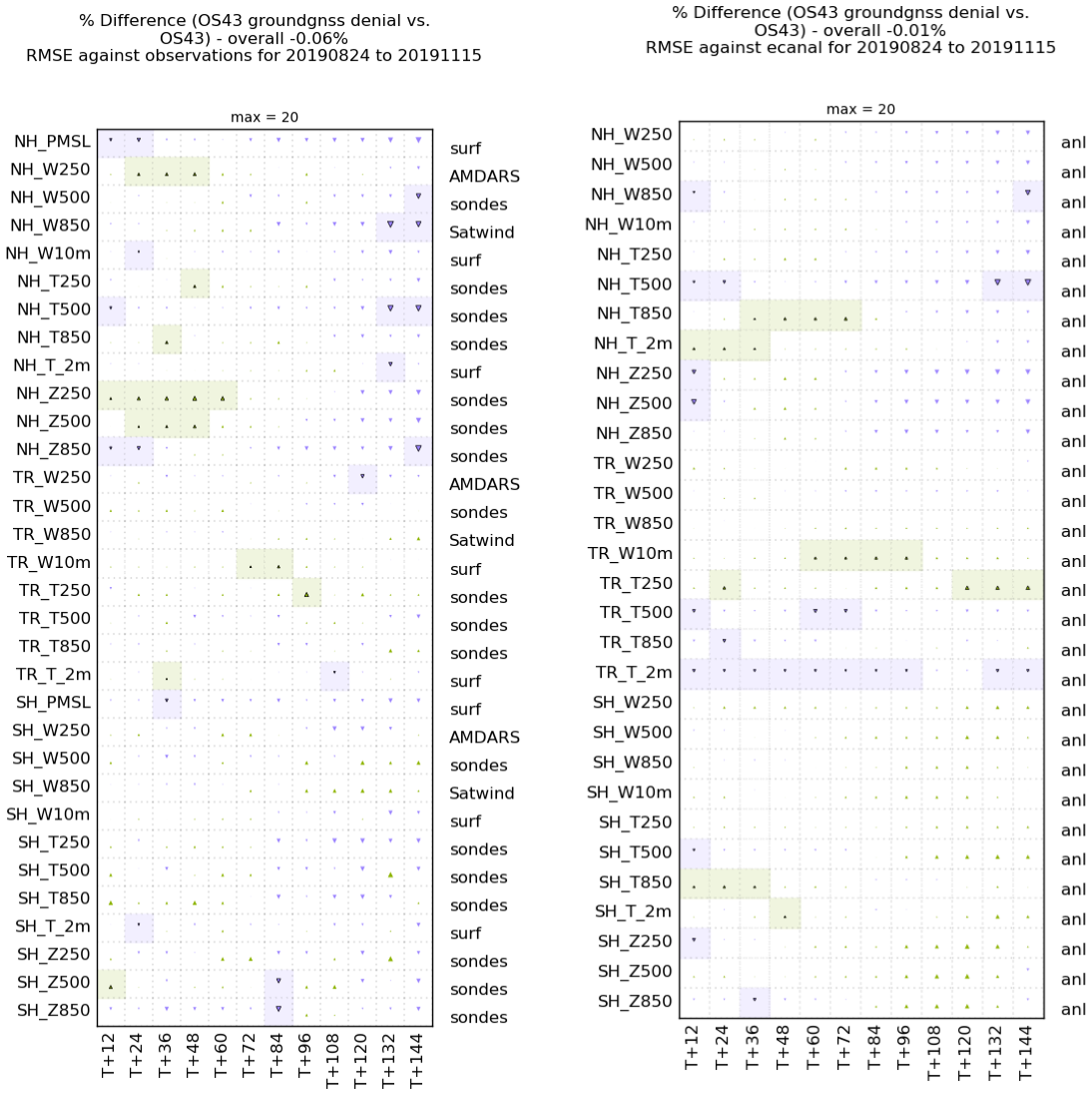

Figure A4 *The change in root mean square forecast error for the Ground-based GNSS data denial experiment. Left Panel: changes verified using observations. right panel: changes verified using ECMWF analyses.*

The largest forecast detriment found in the Ground-based GNSS denial was 0.93% for T+144 NH PMSL (verified by observations).

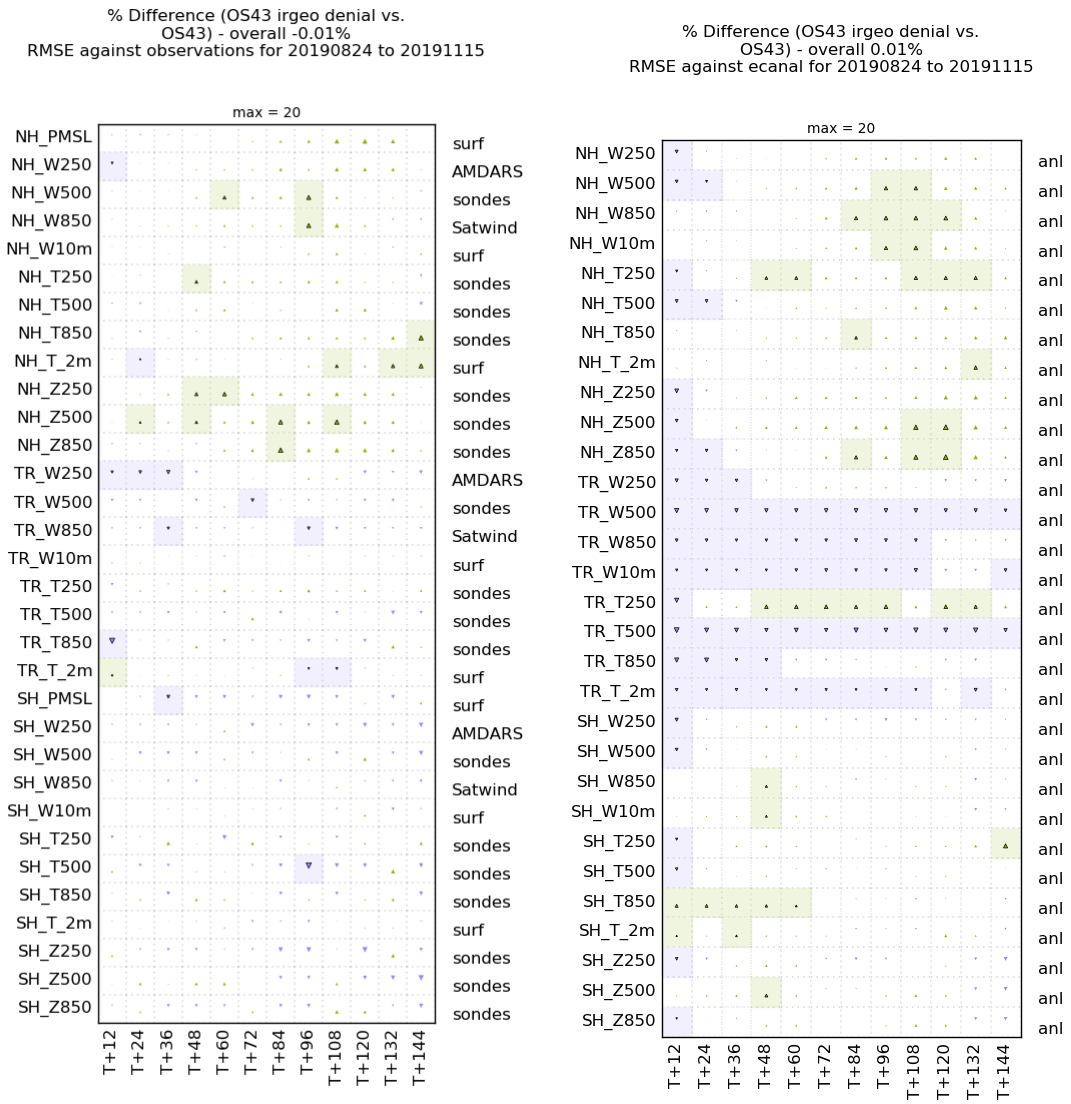

Figure A5 *The change in root mean square forecast error for the Geostationary CSR data denial experiment. Left Panel: changes verified using observations. right panel: changes verified using ECMWF analyses.*

The largest forecast detriment found in the Geostationary CSR denial was 0.78% for T+144 SH_500 hPa height (verified by observations).

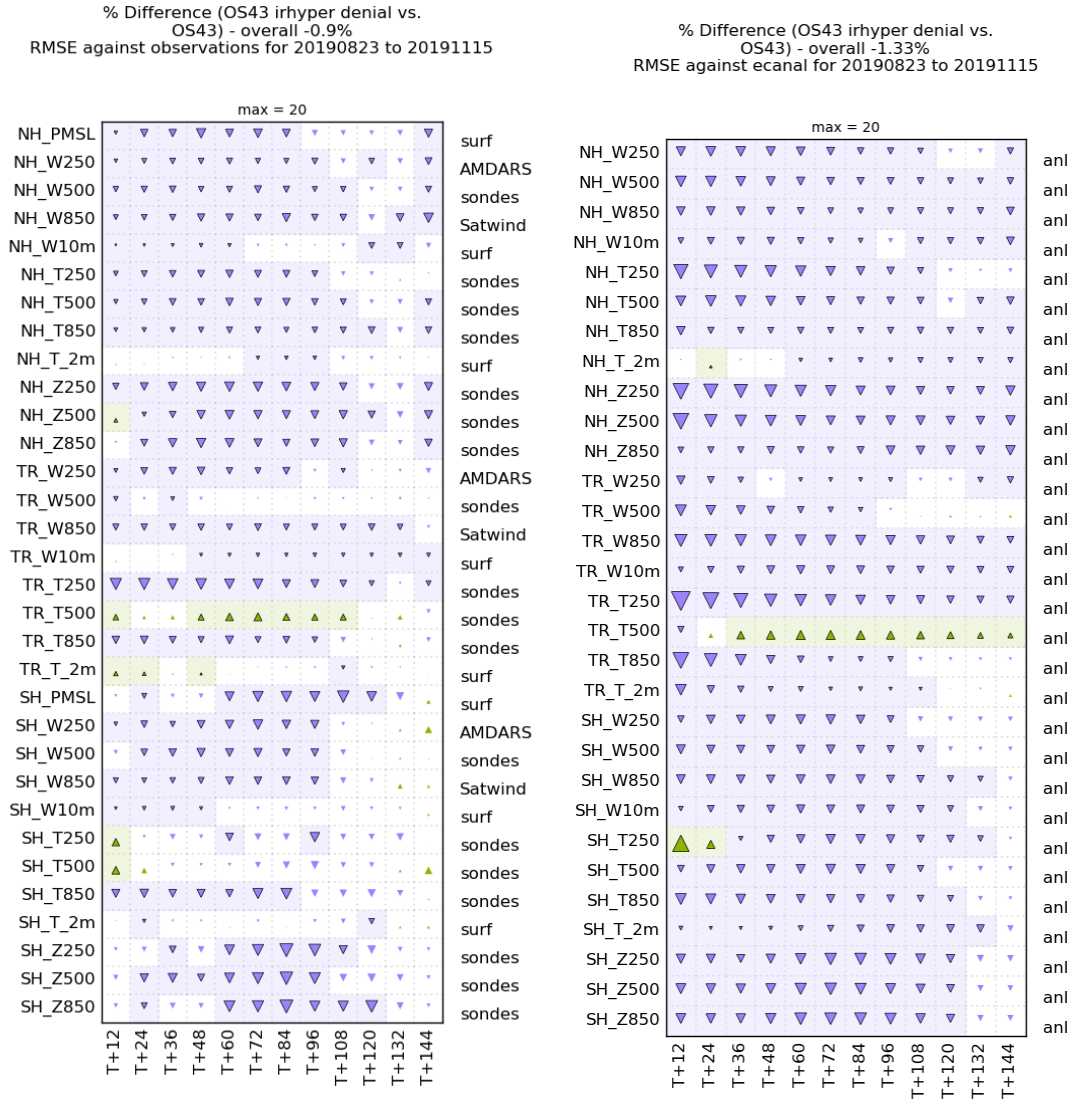

Figure A6 *The change in root mean square forecast error for the Hyperspectral IR data denial experiment. Left Panel: changes verified using observations. right panel: changes verified using ECMWF analyses.*

The largest forecast detriment found in the Hyperspectral IR denial was 7.9% for T+12 TR temperature at_250 hPa (verified by ECMWF analyses).

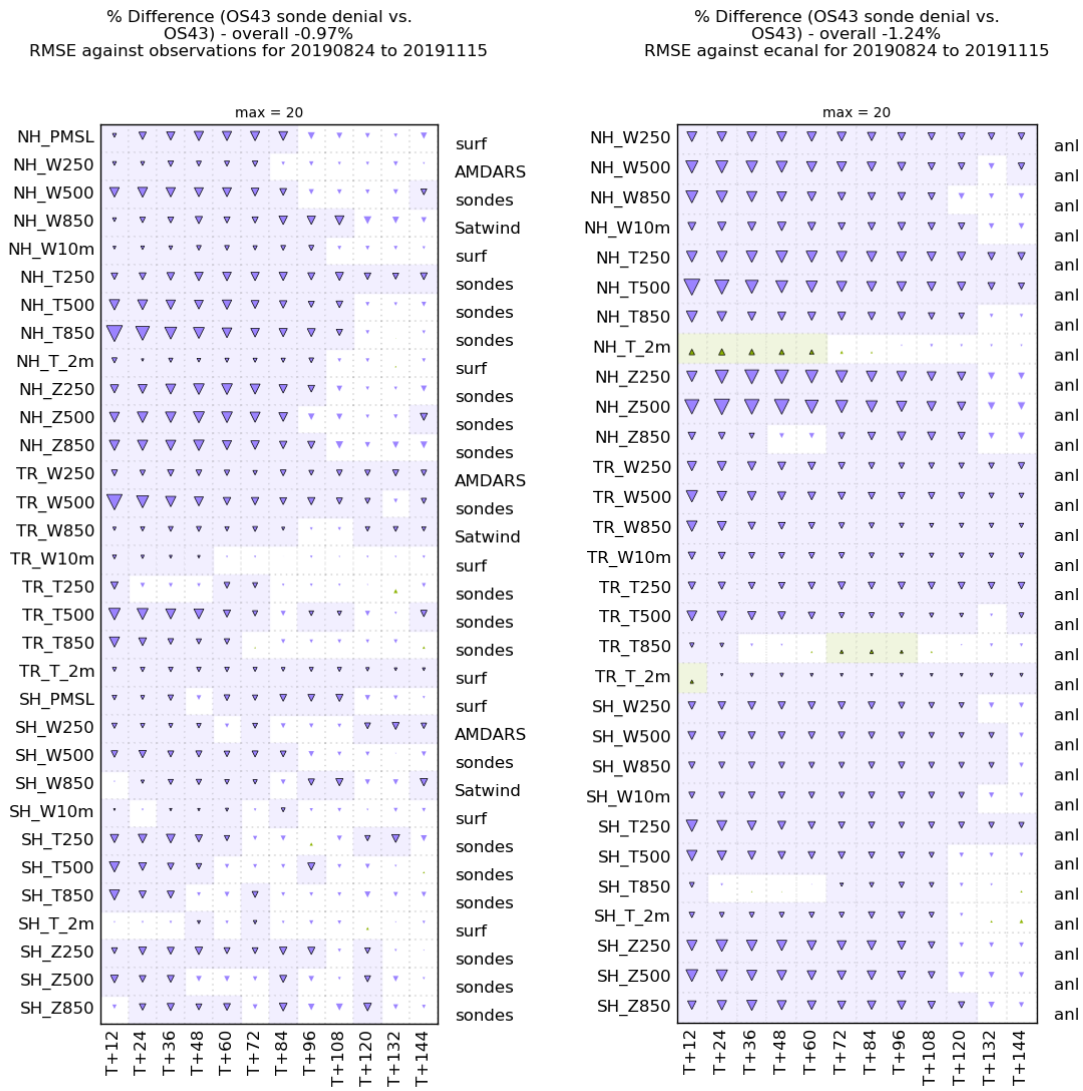

Figure A7 *The change in root mean square forecast error for the Radiosonde data denial experiment. Left Panel: changes verified using observations. right panel: changes verified using ECMWF analyses.*

The largest forecast detriment found in the Radiosonde denial was 6.5% for T+12 NH temperature at_850 hPa (verified by observations)

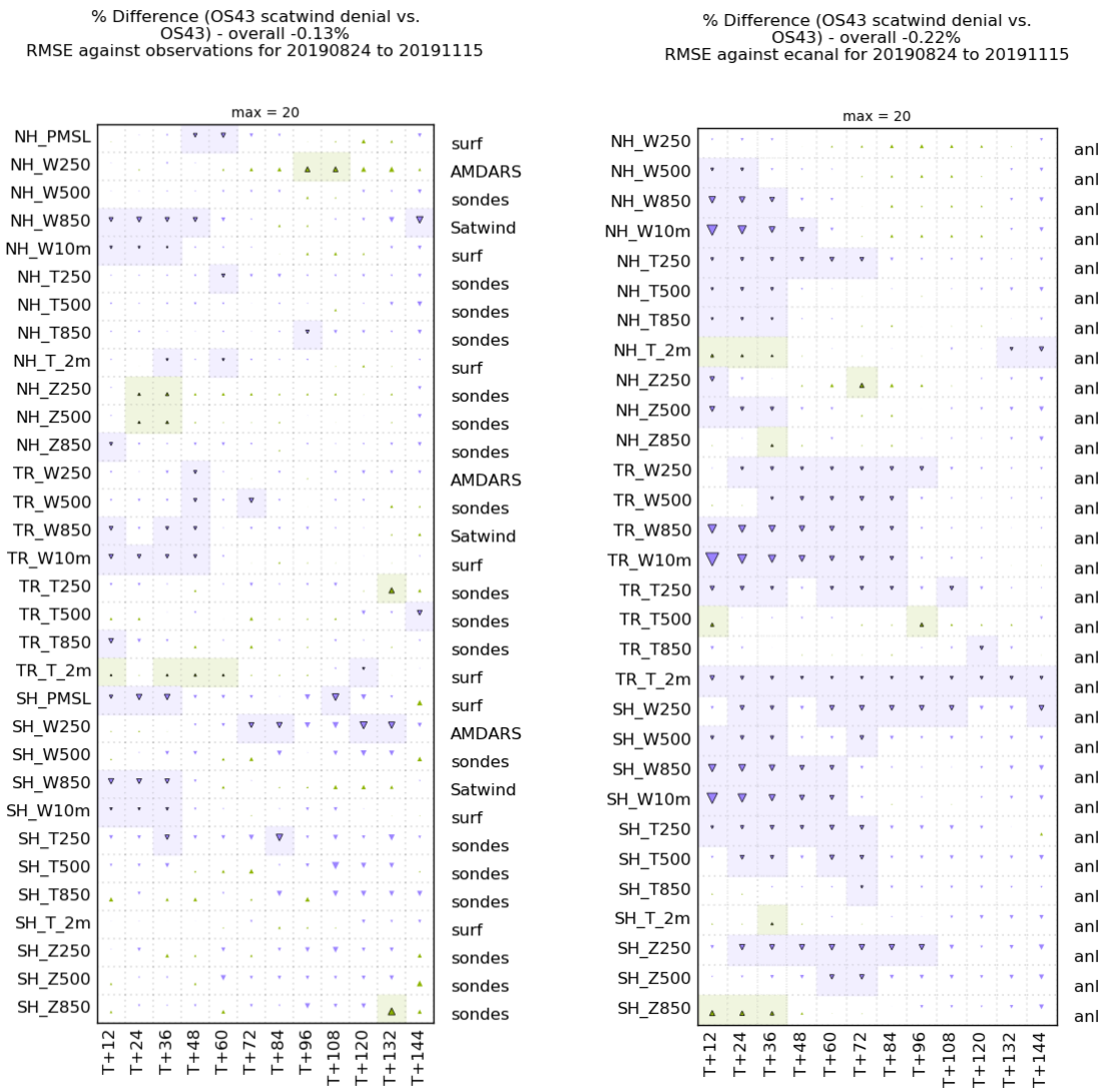

Figure A8 *The change in root mean square forecast error for the Scatwind data denial experiment. Left Panel: changes verified using observations. right panel: changes verified using ECMWF analyses.*

The largest forecast detriment found in the Scatwind denial was 3.8% for T+12 TR winds at 10 m (verified by observations).

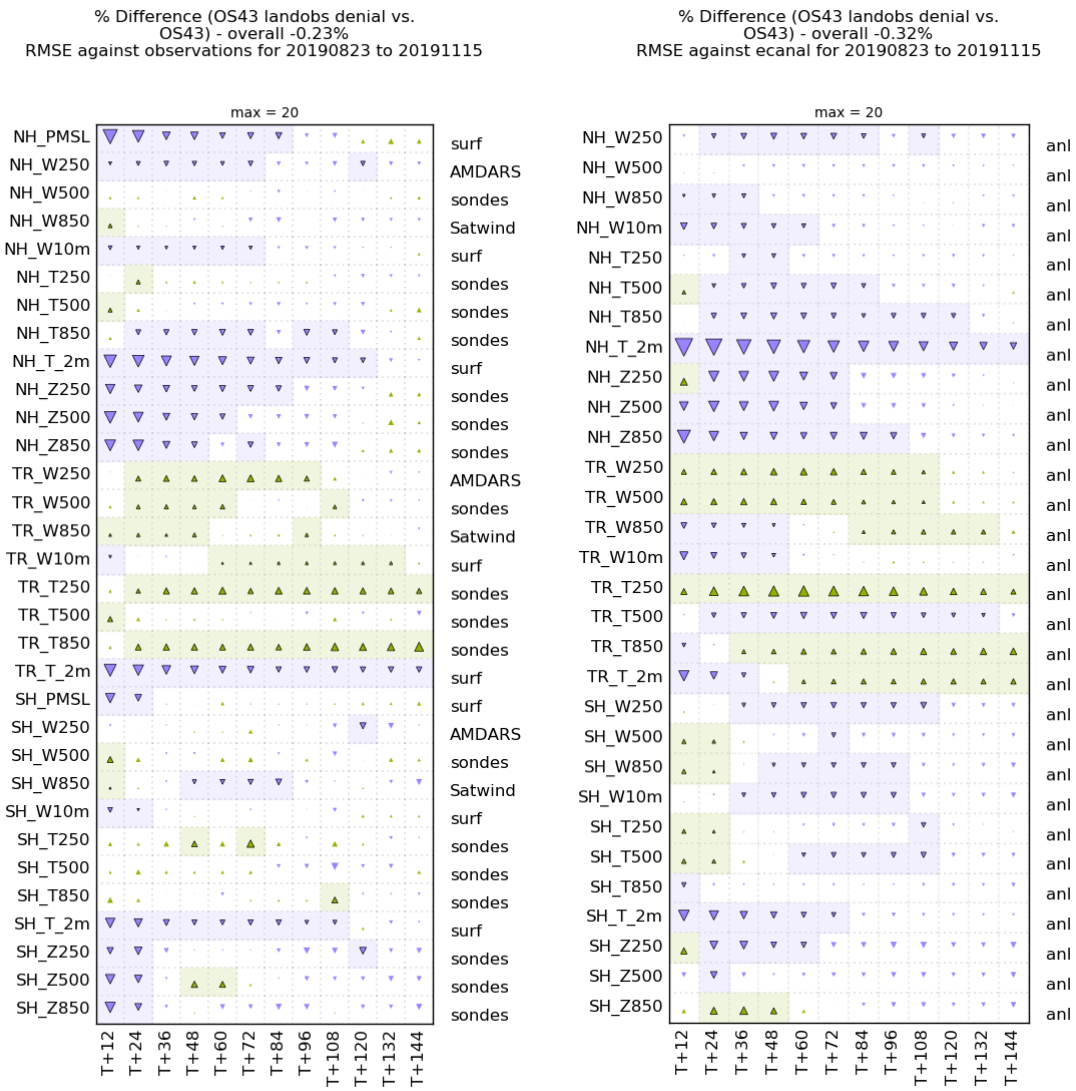

Figure A9 *The change in root mean square forecast error for the Surface-land data denial experiment. Left Panel: changes verified using observations. right panel: changes verified using ECMWF analyses.*

The largest forecast detriment found in the Surface-land denial was 6.9% for T+12 NH temperature at 2 m (verified by observations)

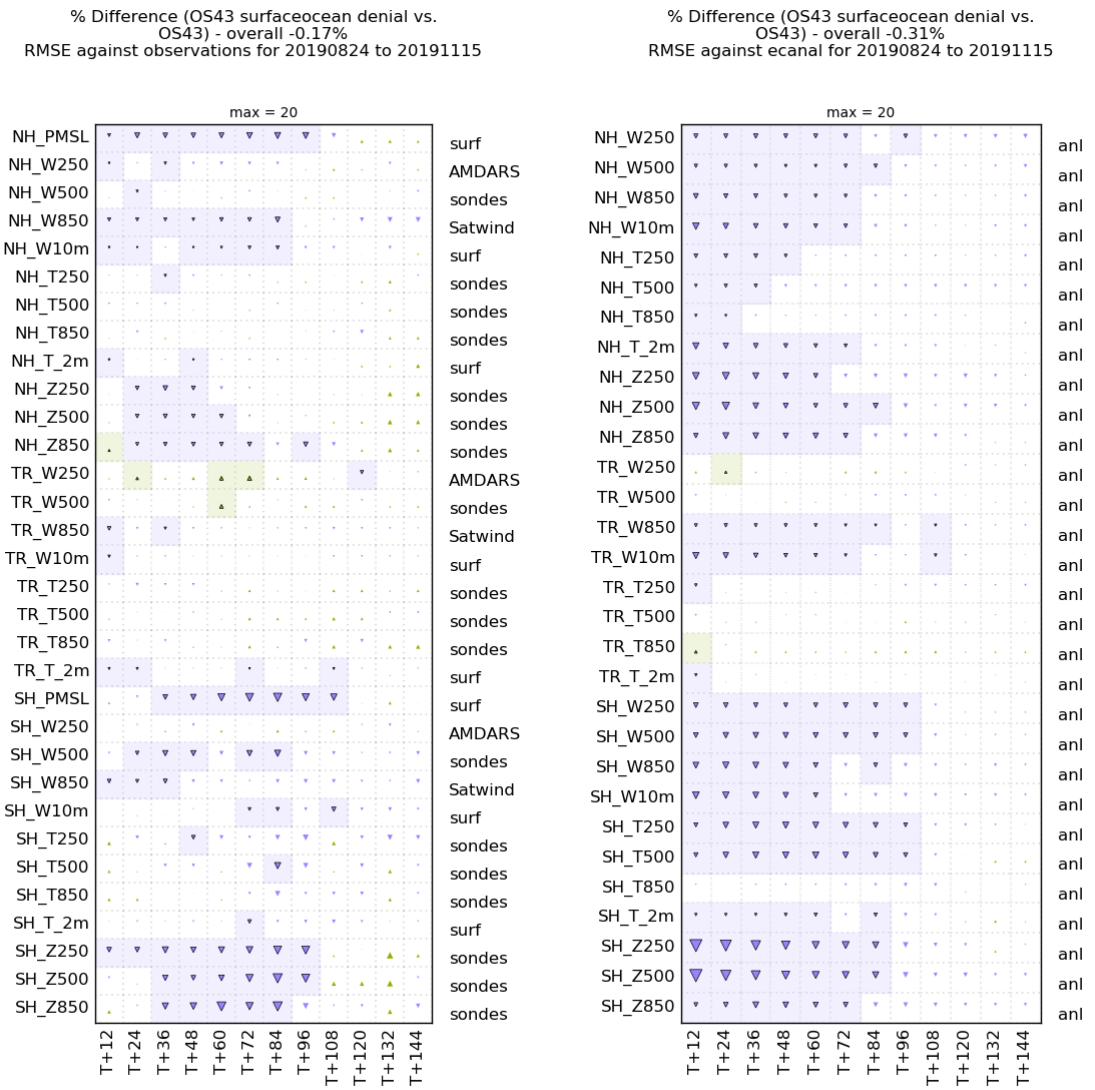

Figure A10 *The change in root mean square forecast error for the Surface-ocean data denial experiment. Left Panel: changes verified using observations. right panel: changes verified using ECMWF analyses.*

The largest forecast detriment found in the Surface-ocean denial was 3.4% for T+12 SH height at 500 hPa (verified by ECMWF).

Met Office
FitzRoy Road
Exeter
Devon
EX1 3PB
United Kingdom